

Giant atomic displacement at a magnetic phase transition in metastable Mn₃O₄S. Hirai,^{1,2} A. M. dos Santos,³ M. C. Shapiro,^{2,4} J. J. Molaison,³ N. Pradhan,³ M. Guthrie,^{3,5} C. A. Tulk,³
I. R. Fisher,^{2,4} and W. L. Mao^{1,2}¹*Department of Geological and Environmental Sciences, Stanford University, California 94305, USA*²*Stanford Institute of Materials and Energy Science, SLAC National Accelerator Laboratory, 2575 Sand Hill Road, Menlo Park, California 94025, USA*³*Oak Ridge National Laboratory, 1 Bethel Valley Road, Oak Ridge, Tennessee 37831, USA*⁴*Geballe Laboratory for Advanced Materials and Department of Applied Physics, Stanford University, Stanford, California 94305, USA*⁵*Carnegie Institution of Washington, 5251 Broadbranch Road, N.W., Washington, D.C. 20015, USA*

(Received 22 October 2012; revised manuscript received 27 December 2012; published 14 January 2013)

We present x-ray, neutron scattering, and heat capacity data that reveal a coupled first-order magnetic and structural phase transition of the metastable mixed-valence postspinel compound Mn₃O₄ at 210 K. Powder neutron diffraction measurements reveal a magnetic structure in which Mn³⁺ spins align antiferromagnetically along the edge-sharing *a* axis, with a magnetic propagation vector $k = [1/2, 0, 0]$. In contrast, the Mn²⁺ spins, which are geometrically frustrated, do not order until a much lower temperature. Although the Mn²⁺ spins do not directly participate in the magnetic phase transition at 210 K, structural refinements reveal a large atomic shift at this phase transition, corresponding to a physical motion of approximately 0.25 Å, even though the crystal symmetry remains unchanged. This “giant” response is due to the coupled effect of built-in strain in the metastable postspinel structure with the orbital realignment of the Mn³⁺ ion.

DOI: [10.1103/PhysRevB.87.014417](https://doi.org/10.1103/PhysRevB.87.014417)

PACS number(s): 61.66.Fn, 61.05.fm, 75.25.-j, 75.47.Lx

I. INTRODUCTION

Large atomic movements can occur at displacive phase transitions. For example, atomic displacements of 0.05–0.4 Å are found for many ferroelectric materials, which lose their inversion symmetry.¹ Typically, atomic displacements are much smaller for isostructural transitions, although it has recently been shown that a “giant” atomic displacement of 0.05–0.09 Å occurs in hexagonal manganites due to large magnetoelastic coupling.² In the present work, we obtain a larger atomic displacement of 0.25 Å at a coupled magnetic and structural phase transition in metastable Mn₃O₄ postspinel. Distinct from simple magnetostriction, this effect is a direct consequence of the highly strained metastable crystal lattice of Mn₃O₄ in the postspinel structure. These results provide a new avenue for the design of materials exhibiting giant atomic displacements without breaking inversion symmetry.

Mn₃O₄ is a unique mixed-valence oxide that adopts a tetragonally distorted spinel structure at ambient conditions.³ This spinel phase undergoes a structural phase transition at 15 GPa into the CaMn₂O₄-type phase, referred to as postspinel (Fig. 1), which is quenched to ambient pressure.^{4,5} The magnetic properties of Mn₃O₄ spinel have been extensively studied, with three magnetic transitions and a pronounced magnetodielectric coupling being reported.^{6,7} On the other hand, studies of Mn₃O₄ postspinel are limited to structural work using x-ray diffraction (XRD)^{4,8} and Raman spectroscopy.⁹ In the present work, we have determined the magnetic structure of Mn₃O₄ postspinel at ambient pressure using neutron diffraction. We find that the onset of long-range magnetic order of the Mn³⁺ moments at $T_N = 210$ K is coupled to a first-order structural transition. The Mn²⁺ moments do not order at T_N due to the intrinsic frustration of the crystal lattice but nevertheless experience a large atomic shift of 0.25 Å. This “giant” effect is due to the exaggerated strain of the Mn²⁺O₈ polyhedra in the metastable postspinel structure.

II. EXPERIMENTAL METHODS

Polycrystalline samples of Mn₃O₄ postspinel were synthesized using a Paris-Edinburgh cell apparatus. Mn₃O₄ spinel was used as a starting material, which was originally prepared by heating MnCO₃ in air at 1400 K for 16 h. The starting material was pressurized up to 20 GPa using a cell fitted with polycrystalline diamond double toroidal anvils,¹⁰ followed by a slow decompression at a rate of 5 GPa/h to ambient pressure. The target pressure was set well above the transition pressure (15 GPa) in order to ensure full transformation of the starting material into the postspinel phase.

Low temperature and room temperature neutron diffraction measurements were conducted at beamline 3 (SNAP) of the Spallation Neutron Source (SNS), Oak Ridge National Laboratory (ORNL), on the recovered sample at elevated temperatures between 290 and 8 K in the *d*-spacing range of 0.5–6 Å. Detailed crystallographic information of Mn₃O₄ postspinel obtained by Rietveld refinement of the crystal and magnetic structures are shown in Tables I and II (at 60 and 290 K). Since the atomic positions of octahedrally coordinated Mn³⁺ ($d^4: t_{2g}^3 e_g^1$) and eightfold coordinated Mn²⁺ ($d^5: t_{2g}^3 e_g^2$) ions are crucial for determining the magnetic structure, we also confirmed the lattice parameters obtained from neutron diffraction using synchrotron XRD. Room temperature XRD data were collected at beamline 16-BMD of the Advanced Photon Source (APS) in Argonne National Laboratory (ANL) using x rays with a wavelength of $\lambda = 0.41222$ Å. GSAS software was used for Rietveld refinement of the crystal and magnetic structures. Lattice constants obtained from the synchrotron XRD measurements were used as a starting model for the neutron diffraction refinement, while the atomic positions obtained from the neutron diffraction were used as a starting model for the XRD refinement, because neutron diffraction has better powder averaging (due to larger beam size) and is more sensitive to the oxygen positions.

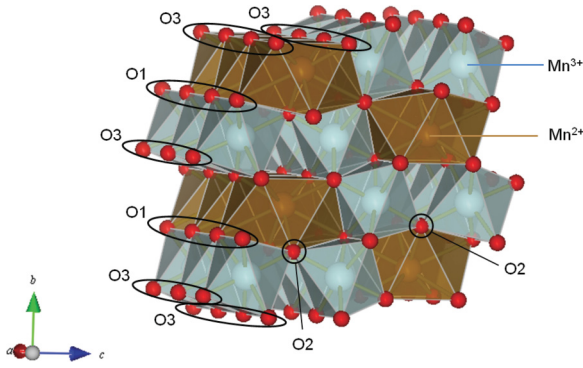


FIG. 1. (Color online) Crystal structure of metastable Mn_3O_4 postspinel [orthorhombic, $Pbcm(57)$] at ambient pressure and room temperature. Gold shading represents the Mn^{2+}O_8 coordination polyhedra, while blue shading represents the Mn^{3+}O_6 octahedra. Large atomic displacements at the magnetic phase transition are a consequence of the built-in strain in this metastable structure.

III. RESULTS AND DISCUSSION

Powder neutron diffraction and XRD refinement at room temperature [Fig. 2(a)] demonstrate that the quenched sample of Mn_3O_4 crystallizes in the CaMn_2O_4 -type postspinel structure with $Pbcm$ space group as anticipated following previous reports.⁴ The lattice parameters obtained by these two methods were consistent, the difference being within the standard deviation. The room-temperature crystal structure, in which Mn^{3+}O_6 octahedra form one-dimensional edge-sharing chains along the a axis and zigzag along the b axis, is shown in Fig. 1. Eightfold coordinated Mn^{2+} ($d^5: t_{2g}^3 e_g^2$) ions are situated in the cavity provided by the zigzag connectivity of the

Mn^{3+}O_6 octahedra. Detailed crystallographic data of atomic coordinates and bond lengths and angles are shown in Table I. In particular, we note that at room temperature, the Mn^{3+}O_6 octahedron comprises two short, two medium, and two long $\text{Mn}^{3+}\text{-O}$ bond distances due to the anisotropic connectivity of the coordination-octahedra.

Powder neutron diffraction measurements at low temperature reveal a coupled magnetic and structural phase transition at $T_N = 210$ K. Magnetic peaks were found by excluding the nuclear peaks (< 3 Å), and the propagation vector of $k = [1/2, 0, 0]$ for the magnetic unit cell was found to have the best fit using supercell in FullProf software [representative data shown in Fig. 2(b) for a temperature of 60 K]. In other words, below 210 K, Mn_3O_4 postspinel adopts an a -axis doubled magnetic unit cell [Fig. 2(d)], in which Mn^{3+} spins are aligned antiferromagnetically along the edge sharing a axis. Refinement was performed based on this magnetic unit cell in the $Pbca$ space group, yielding an ordered moment for the Mn^{3+} spins of $\mu_x = 3.49(2) \mu_B$ at 60 K (moment along the crystallographic a axis). The temperature dependence of the ordered moment, shown in Fig. 4(a), exhibits a rapid drop at $T_N = 210$ K, indicative of a first-order phase transition. In contrast, as described in greater detail below, the Mn^{2+} moments do not appear to order at T_N , but remain paramagnetic down to approximately 50 K. Based on the refinement results described above, the temperature-dependence of the lattice parameters was also determined for a cooling cycle down to 8 K. For the lattice constants a and b , a discontinuity around 210 K is clearly observed [Figs. 3(a) and 3(b)], signaling a coupled first-order structural phase transition, which is accompanied by a lattice volume drop of 0.5(1)%. In spite of the considerable volume drop, this transition does not change the original $Pbcm$ symmetry and the material retains its inversion symmetry.

Heat capacity (C_p) measurements were made for similar polycrystalline samples of Mn_3O_4 postspinel between 2 and 290 K, and representative data are shown in Fig. 4(a). These measurements reveal a broad feature near 210 K, supporting the x-ray and neutron scattering evidence for a phase transition. The width of the “peak” in the heat capacity at this transition likely reflects the presence of inhomogeneous strain quenched from the high pressure synthesis. A similar broadening of an otherwise sharp first-order transition has been observed for polycrystalline samples of other spinel compounds, such as MnV_2O_4 .¹¹

Mn^{2+} ions occupy an inequivalent site to Mn^{3+} in the Mn_3O_4 crystal lattice. Consequently, any magnetic order associated with the Mn^{2+} ions must either lead to additional diffraction peaks for a $Q \neq 0$ structure or an enhancement of the nuclear peaks for a $Q = 0$ structure. Neither effect is observed down to 55 K, and we conclude that the Mn^{2+} ions do not order until the lower temperature. This effect can be attributed to geometric frustration since the Mn^{2+} ions are situated at the center of a honeycomb arrangement of Mn^{3+} spins that are antiferromagnetically ordered [illustrated in Fig. 2(e)]. However, at 55 K an additional feature is seen in the heat capacity [Fig. 4(a)], suggesting an additional phase transition. The crystal lattice does not change appreciably at this temperature, nor does the magnetic structure of the Mn^{3+} moments. However, neutron diffraction data reveal new broad and asymmetric magnetic peaks around 1.8 Å,

TABLE I. Table of crystallographic information of Mn_3O_4 postspinel for representative temperatures above (290 K) and below (60 K) $T_N = 210$ K.

Parameters	60 K	290 K
a (Å)	3.032(1)	3.020(2)
b (Å)	9.842(6)	9.880(4)
c (Å)	9.568(4)	9.583(3)
V (Å ³)	284.4(1)	287.0(1)
$\text{Mn}^{3+}: x$	0.308(8)	0.280(8)
$\text{Mn}^{3+}: y$	0.114(2)	0.114(2)
$\text{Mn}^{3+}: z$	0.070(3)	0.070(3)
$\text{Mn}^{3+}: U_{\text{iso}}$	0.170(4)	0.106(7)
$\text{Mn}^{2+}: x$	0.760(8)	0.876(4)
$\text{Mn}^{2+}: y$	0.137(3)	0.137(3)
$\text{Mn}^{2+}: U_{\text{iso}}$	0.018(5)	0.018(5)
O1: x	0.824(6)	0.824(4)
O1: U_{iso}	0.0064	0.0064
O2: x	0.332(4)	0.340(4)
O2: y	0.194(2)	0.194(2)
O2: U_{iso}	0.0064	0.0064
O3: x	0.800(2)	0.724(2)
O3: y	0.968(1)	0.968(1)
O3: z	0.105(2)	0.105(2)
O3: U_{iso}	0.0064	0.0064
R_{wp}	0.0246	0.0258

TABLE II. Bond angles for representative temperatures above (290 K) and below (60 K) $T_N = 210$ K.

T (K)	Mn ³⁺ -O2-Mn ³⁺	O1-Mn ³⁺ -O1	O1-Mn ³⁺ -O2	O1-Mn ³⁺ -O3	O2-Mn ³⁺ -O3	O3-Mn ³⁺ -O3
290	129.7(3)	90.6(1)	86.6(1), 97.1(5)	84.5(3), 84.6(1), 92.5(6), 94.5(1)	91.8(5), 102.5(5)	76.2(3), 86.7(4), 90.8(1)
60	130.7(9)	90.4(1)	89.8(5), 92.7(6)	82.4(4), 88.0(5), 88.8(5), 96.7(3)	96.4(8), 99.2(6)	74.2(5), 88.7(6), 91.3(4)

4.5 Å, 4.9 Å, and 5.1 Å [Fig. 2(c)]. The d spacing of these peaks is not consistent with the Mn³⁺ moments and indeed the T dependence of the magnetic Bragg peaks associated with the Mn³⁺ sublattice evolve smoothly down to 8 K. The d spacing of the additional magnetic peaks are, however, consistent with the ordering of the Mn²⁺ moments. Since these peaks are incommensurate with the nuclear Bragg peaks [Fig. 2(c)] it appears that the Mn²⁺ moments adopt an incommensurate finite Q magnetic structure. However, the broad and asymmetric character of these peaks also implies that the associated correlation length is not especially long and hence might be better characterized as short-range order.

The paramagnetic behavior of Mn²⁺ spins above 55 K is evident from susceptibility measurements (Fig. 5). In comparison to CaMn₂O₄, for which the susceptibility monotonically decreases as the temperature is reduced below T_N , Mn₃O₄ reveals a susceptibility that increases upon cooling (upper inset to Fig. 5). The data can be fit to the sum

of a temperature-independent term and a Curie-Weiss term [i.e., $\frac{1}{\chi} = (\chi_0 + \frac{C}{T-\theta})^{-1}$] yielding an effective moment $\mu_{\text{eff}} = 2.32(2) \mu_B$ per formula unit in the temperature range between 100 and 200 K. This value should be treated with a certain amount of caution. The ordered lattice of Mn³⁺ moments will not give a temperature-independent susceptibility, and hence μ_{eff} does not provide a perfect measure of the actual effective moment of paramagnetic Mn²⁺ spins (for which one anticipates $\mu_{\text{eff}} = 5.92 \mu_B$).

At low temperatures, the susceptibility of Mn₃O₄ rises rapidly and exhibits a clear hysteresis between field cooled (FC) and zero-field cooled (ZFC) measurements, both of which are consistent with the onset of ferromagnetism. The magnetization (Fig. 6) also exhibits a clear remnance for temperatures below $T_C \sim 55$ K. Evidently, the incommensurate short-range magnetic order inferred from neutron diffraction measurements has a ferromagnetic component. The magnetization does not saturate in fields up to 5 T, but since the measurements were made for polycrystalline samples, we cannot comment on the origin of this effect.

The small changes in lattice parameter and unit cell volume at T_N mask some startlingly large atomic displacements within the unit cell. Atomic coordinates and the associated bond lengths and angles are shown in Table I for representative temperatures above (290 K) and below (60 K) T_N . Focussing first on the Mn³⁺O₆ coordination octahedra, the structural transition involves a relatively large motion of the O3 oxygen ion, with a change of 5% in the unit cell coordinate, corresponding to a displacement of 0.16 Å. This motion leads to a smaller distortion of the octahedron in the xy plane relative to the room temperature structure, such that at low temperatures the four coordinating oxygen ions in the xy plane form an almost perfect square (Fig. 7). The corresponding change in the orbital character of the Mn³⁺ ion affects the magnitude of the exchange interaction between nearest neighbor Mn³⁺ ions, possibly providing the driving force for the O3 ionic motion.

Surprisingly, our refinements also reveal a very large atomic shift along the a axis for the Mn²⁺ ions [Fig. 4(b)] at T_N . The unit cell coordinate changes by 8%, corresponding to a displacement of 0.25 Å, *even though these ions do not directly participate in the magnetic phase transition*. This effect is even larger than that found in giant magnetoelastic compounds such as hexagonal manganites (atomic displacement: 0.05–0.09 Å).² However, in the case of Mn₃O₄ the effect does not arise directly from magnetoelastic coupling, because the Mn²⁺ ions do not directly participate in the magnetic phase transition. The origin of this effect is intimately linked to the metastable nature of Mn₃O₄ in the postspinel structure at ambient pressure, and in particular to the severely strained Mn²⁺O₈ polyhedra. Mn₃O₄ postspinel is isostructural with CaMn₂O₄, which is thermodynamically stable, but the Mn²⁺ ion is much smaller than Ca²⁺. As a result, the Mn²⁺O₈ polyhedron is

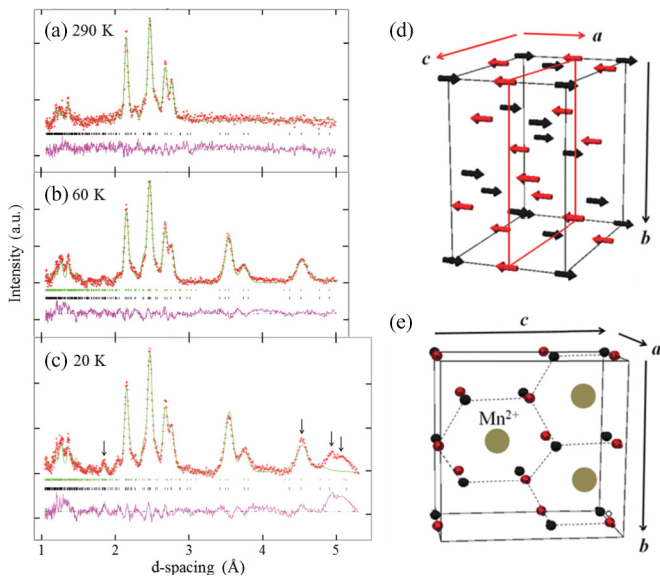


FIG. 2. (Color online) Neutron powder diffraction profile of Mn₃O₄ postspinel at (a) 290 K and (b) 60 K. Magnetic Bragg peaks are indicated by green marks, while nuclear Bragg peaks are indicated by black marks. The pink curve represents the difference between the observed and calculated neutron diffraction intensities based upon the refined magnetic structure described in the main text. (c) Magnetic structure for Mn³⁺ spins in Mn₃O₄ (arrows represent Mn³⁺ spins: black arrows are the spins parallel to the spin at the origin, while red arrows are the spins antiparallel to the spin at the origin). (d) Magnetic frustration of the Mn²⁺ spins against the antiferromagnetically ordered Mn³⁺ spins (black signs point out of the paper, while red signs point into the paper). The gold sphere represents the Mn²⁺ ion, which is situated at the center of the honeycomb composed of six antiferromagnetically ordered Mn³⁺ spins.

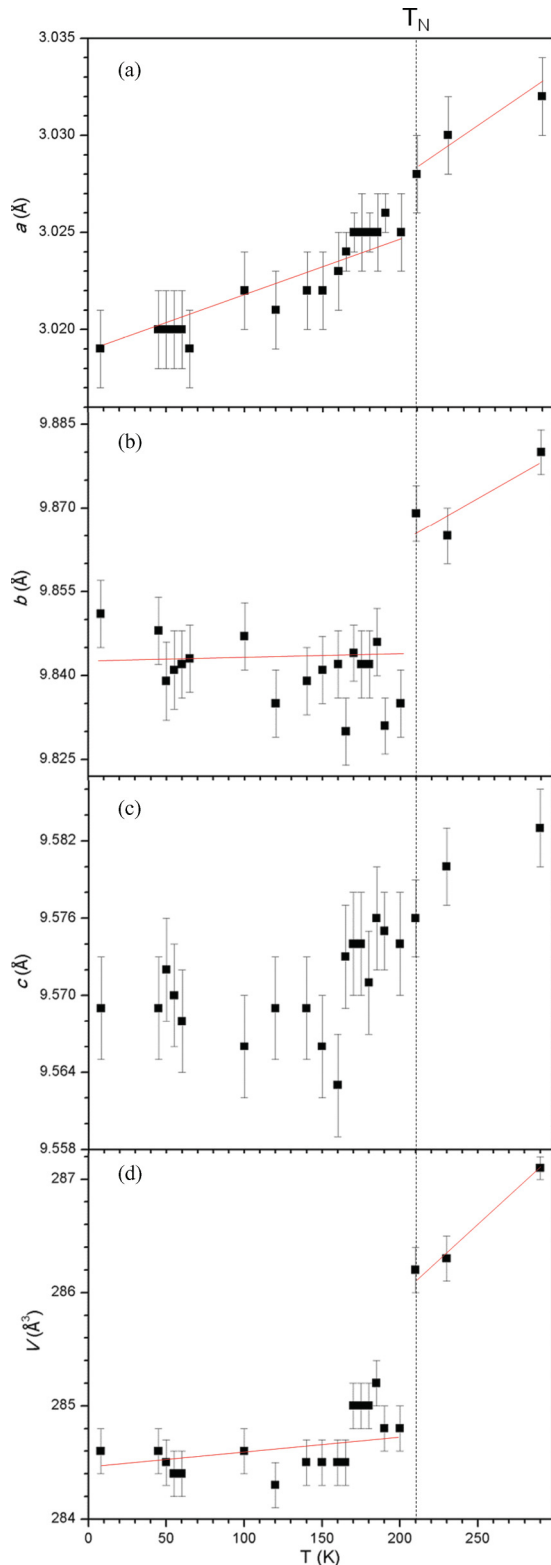


FIG. 3. (Color online) Temperature dependence of lattice constants (a) a , (b) b , (c) c , and (d) unit cell volume for Mn_3O_4 postspinel. Vertical lines at 210 K indicate the coupled magnetic and structural phase transition.

considerably stretched relative to the ideal bond lengths. This is borne out by the bond valence sum (BVS), which is 1.82, smaller than the formal valence 2. The associated strain is

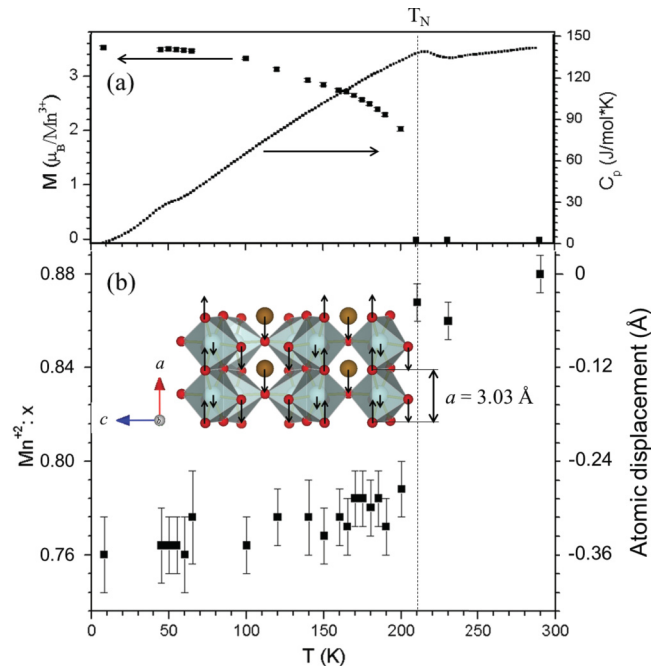


FIG. 4. (Color online) Temperature dependence of (a) the magnetic moment of Mn^{3+} (left axis) and the specific heat C_p (right axis); and (b) the atomic position of Mn^{2+} in Mn_3O_4 postspinel, expressed on the left axis in terms of the atomic coordinate x in the unit cell and on the right axis in terms of the actual atomic displacement relative to the position at 290 K. Dashed vertical line indicates approximate transition temperature. Inset shows the atomic displacements at 200 K found upon cooling below $T_N = 210$ K for Mn^{2+} (8% shift in unit cell coordinates, corresponding to 0.25 Å) and O3 (5% shift in unit cell coordinates, corresponding to 0.16 Å) represented by black arrows. The much smaller atomic displacement of Mn^{3+} (2% shift in unit cell coordinates, corresponding to 0.06 Å) due to the magnetoelastic coupling is also shown. The directions of atomic displacement shown in the figure are only the representative ones, and equal number of atoms move in the opposite directions due to the $Pbcm$ symmetry. The arrows are illustrated in proportional length to the atomic displacements of Mn^{2+} , O3, and Mn^{3+} but are all exaggerated by a factor of 4 for clarity.

rather severe and can act to magnify the effects of more modest ionic displacements at the magnetic phase transition. Specifically, on cooling below T_N , the associated change in position of the O3 ions described above would result in a further reduction of the BVS of the Mn^{2+} ions if they did not move. Indeed, if the Mn^{2+} ions did not move at T_N , the BVS would change from 1.83 to 1.73, far below the optimal value of 2 associated with the formal 2+ valence. Consequently, in order to minimize the elastic energy, the Mn^{2+} ions experience a giant atomic displacement, recovering a low-temperature BVS of 1.83, closer to the expected value. Such a large atomic shift of Mn^{2+} suggests that Mn_3O_4 postspinel is at the edge of the phase boundary between the postspinel and the spinel phase and is therefore highly susceptible to large atomic displacements.

Since Mn_3O_4 postspinel is isostructural with CaMn_2O_4 , and the only chemical difference is that Ca^{2+} is replaced by Mn^{2+} , it is instructive to compare the physical properties of these two compounds. Mn_3O_4 exhibits an insulating behavior similar to CaMn_2O_4 ¹² with a very large resistivity.

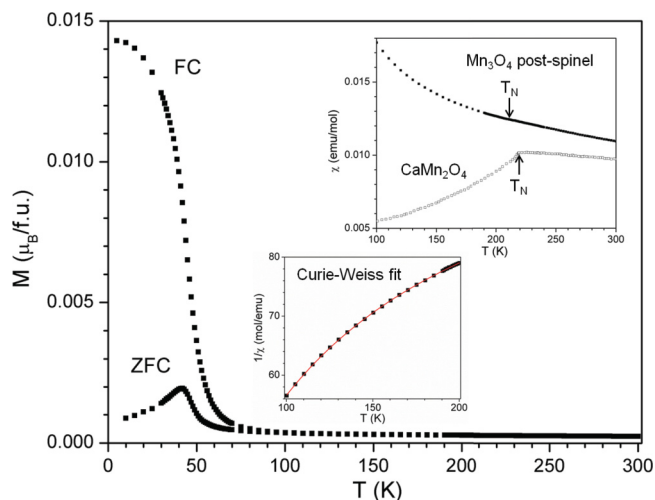


FIG. 5. (Color online) Zero field-cooled (ZFC) and field-cooled (FC) magnetic susceptibility (M/H) curve for Mn_3O_4 postspinel measured in a field of 100 Oe. Upper inset shows the comparison of the ZFC magnetic susceptibility for Mn_3O_4 postspinel (represented by black squares) with that for CaMn_2O_4 (represented by open squares) in the temperature regime of $100 < T < 300$ K (for comparison, both samples are measured in a field of 2000 Oe). ZFC magnetic susceptibility for CaMn_2O_4 was taken from Ref. 12. Lower inset shows the inverse susceptibility between 100 and 200 K for Mn_3O_4 postspinel, which can be fitted using the equation $\frac{1}{\chi} = (\chi_0 + \frac{C}{T-\theta})^{-1}$, combining temperature-independent and Curie-Weiss terms [$\chi_0 = 0.00886(3)$ (emu mol $^{-1}$), $C = 0.668(9)$ (emu K mol $^{-1}$), $\theta = 24.2(8)$ (K)]. The Curie constant C gives $\mu_{\text{eff}} = 2.32(2) \mu_B$.

CaMn_2O_4 exhibits long-range antiferromagnetic order below $T_N = 217$ K,¹² comparable to that of Mn_3O_4 , and also adopts the same magnetic structure as the Mn^{3+} spins for Mn_3O_4 . However, in contrast with Mn_3O_4 postspinel, the magnetic phase transition in CaMn_2O_4 is continuous and the associated

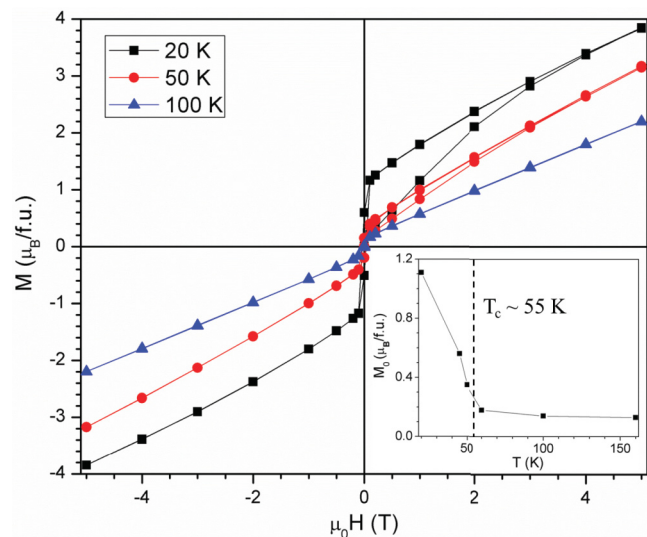


FIG. 6. (Color online) Magnetic hysteresis loops measured at $T = 20$ K (square), $T = 50$ K (triangle), and $T = 100$ K (circle) for Mn_3O_4 postspinel. The inset shows the temperature dependence of the zero-field magnetization M_0 obtained by a fourth-order polynomial extrapolation of the magnetization at high field.

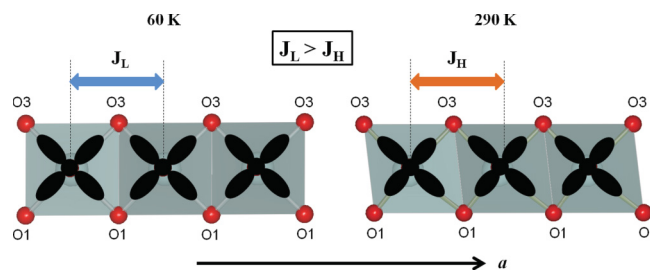


FIG. 7. (Color online) Schematic view of the edge-sharing Mn^{3+}O_6 octahedra along the a axis at 60 K (below T_N) and at 290 K (above T_N). Blue shading represents the coordination octahedra, and red spheres represent the oxygen ions. The associated $d_{x^2-y^2}$ orbitals are shown in black. Above T_N , $d_{x^2-y^2}$ and $d_{3z^2-r^2}$ orbitals are mixed and d orbitals partially align along the longest bonds of the Mn^{3+}O_6 octahedron. The Mn^{3+}O_6 octahedra are less distorted in the xy plane below T_N . The associated change in the orbital character leads to an enhanced exchange interaction along the a axis.

atomic displacements of Ca^{2+} and $\text{O}3$ ions are considerably smaller (the corresponding differences in atomic positions between 300 K and 20 K are just 0.012 Å for Ca^{2+} , and 0.003 Å for $\text{O}3$ ¹³, relative to 0.25 Å and 0.16 Å for Mn^{2+} and $\text{O}3$ ions in Mn_3O_4 postspinel). The origin of this difference lies in the metastable nature of postspinel Mn_3O_4 . CaMn_2O_4 is a thermodynamically stable phase, and the specific crystal lattice is a minimum of the free energy. The lattice is relatively stiff, and associated motion of $\text{O}3$ ions in response to the onset of long-range magnetic order is correspondingly small. However, the built-in strain associated with the metastable postspinel structure adopted by Mn_3O_4 quenched from high-pressure leads to a softer crystal lattice, and hence an exaggerated response of both the $\text{O}3$ and Mn^{2+} ions to the onset of long-range magnetic order. Figure 8 shows the comparison of our heat capacity data of Mn_3O_4 postspinel with the previously reported heat capacity of CaMn_2O_4 .¹² Apart from the peak

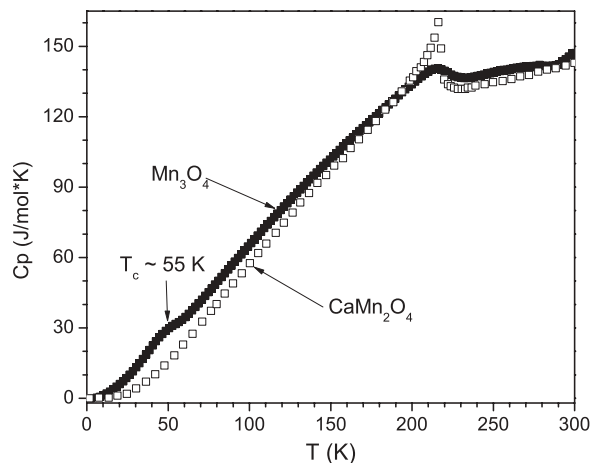


FIG. 8. The comparison of specific heat (C_p) of Mn_3O_4 postspinel (represented by black squares) with C_p of CaMn_2O_4 (represented by open squares) in the temperature regime of $0 < T < 300$ K. The specific heat data of CaMn_2O_4 was taken from Ref. 12. The ferromagnetic transition at $T_C \sim 55$ K associated with Mn^{2+} moments is indicated by an arrow. This transition is absent for CaMn_2O_4 .

broadening near 215 K due to the strain effect, the only significant difference is found at temperatures lower than 55 K due to the onset of magnetic ordering associated with the Mn^{2+} moments.

IV. CONCLUSION

In conclusion, Mn_3O_4 in the postspinel structure at ambient pressure undergoes an isostructural coupled magnetic and structural phase transition at $T_N = 210$ K. The built-in strain associated with the metastable structure leads to a “giant” atomic displacement of the Mn^{2+} ions at T_N , even though they do not directly participate in the magnetic order due to the effects of geometric frustration. This novel effect illustrates an alternative avenue to achieve giant atomic displacements coupled to magnetic phase transitions.

ACKNOWLEDGMENTS

This research is funded by the US Department of Energy (DOE), Office of Basic Energy Sciences (BES). S.H., W.L.M., M.S., and I.R.F. are supported by the US Department of Energy (DOE), Office of Basic Energy Sciences (BES), Division of Materials Sciences and Engineering, under Contact No. DE-AC02-76SF00515. M.G. is supported by EFree, an Energy Frontier Research Center funded by DOE-BES. Neutron diffraction experiments at the SNAP facility were supported by SNS and Center of Nanophase Materials Science of ORNL. XRD experiments were performed at HPCAT, APS, ANL. HPCAT is supported by CIW, CDAC, UNLV, and LLNL through funding from DOE-NNSA, DOE-BES, and NSF. APS is supported by DOE-BES, under Contract No. DE-AC02-06CH11357. We thank D. Ikuta and W. Yang for help with the XRD experiments.

¹R. W. Wyckoff, *Crystal Structures* (Krieger Publishing, New York, 1986).

²S. Lee, A. Pirogov, M. Kang, K-H. Jang, M. Yonemura, T. Kamiyama, S-W. Cheong, F. Gozzo, N. Shin, H. Kimura, Y. Noda, and J-G. Park, *Nature (London)* **451**, 805 (2008).

³G. Aminoff, *Z. Kristallogr.* **64**, 475 (1927).

⁴E. Paris, C. R. II Ross, and H. Olijnyk, *Eur. J. Mineral.* **4**, 87 (1992).

⁵M. Merlini, M. Hanfland, M. Gemmi, S. Huotari, L. Simonelli, and P. Strobel, *Am. Mineral.* **95**, 200 (2010).

⁶T. Suzuki and T. Katsufuji, *Phys. Rev. B* **77**, 220402 (2008).

⁷R. Tackett, G. Lawes, B. C. Melot, M. Grossman, E. S. Toberer, and R. Seshadri, *Phys. Rev. B* **76**, 024409 (2007).

⁸Y. Moritomo, Y. Ohishi, A. Kuriki, E. Nishibori, M. Takata, and M. Sakata, *J. Phys. Soc. Jpn.* **72**, 765 (2003).

⁹X-J. Liu, S. Xu, K. Kato, and Y. Moritomo, *J. Phys. Soc. Jpn.* **71**, 2820 (2002).

¹⁰S. Klotz, J. M. Besson, G. Hamel, R. J. Nelmes, and J. S. Loveday, *Appl. Phys. Lett.* **66**, 1735 (1995).

¹¹H. D. Zhou, J. Lu, and C. R. Wiebe, *Phys. Rev. B* **76**, 174403 (2007).

¹²B. D. White, J. A. Souza, C. Chiorescu, J. J. Neumeier, and J. L. Cohn, *Phys. Rev. B* **79**, 104427 (2009).

¹³C. D. Ling, J. J. Neumeier, and D. N. Argyriou, *J. Solid State Chem.* **160**, 167 (2001).